Wave tank simulations using a fractional-step method in a cell-centered Finite Volume Implementation

Stefan Mayer, Antoine Garapon and Lars Sørensen
International Research Centre for Computational Hydrodynamics (ICCH),
Agern Allé 5, DK-2970 Hørsholm, Denmark, e-mail: icch@dhi.dk

Introduction. Many attempts have been made in the past to solve the unsteady incompressible Euler or Navier Stokes equations with full nonlinear free surface description, without the assumption of irrotational flow and use of the Bernoulli type dynamic boundary condition. Unfortunately, it seems that these methods usually have suffered from relatively large numerical errors and especially numerical damping, which did not allow accurate long term simulations of travelling gravity waves, see e.g. Tsai and Yue (1996) [4].

Here, an attempt is made to extend the application range of free surface Euler equations, so that unsteady wave problems can be simulated with accuracies, which are comparable to those of potential flow methods. In the present paper, the method has been applied to travelling waves in channels with submerged bars, and results are compared to experimental data. Furthermore, steady currents are introduced and wave current interaction is described, including wave blocking conditions.

Method. The two-dimensional Euler equations,

$$\nabla \cdot \boldsymbol{u} = 0, \tag{1}$$

$$\frac{\partial \boldsymbol{u}}{\partial t} + \boldsymbol{u} \cdot \nabla \boldsymbol{u} = -\nabla p, \tag{2}$$

are solved for the Cartesian velocity $\boldsymbol{u} = (u_x, u_y)$ and dynamic pressure p. The usual inviscid dynamic boundary conditions are imposed,

$$p = \rho g \eta \ , \quad \nabla \boldsymbol{u} \cdot \boldsymbol{n} = 0, \tag{3}$$

η denoting the free surface elevation and $\boldsymbol{n}$ being the surface normal vector. The kinematic boundary condition is expressed in terms of the local volume flux $f = \boldsymbol{u} \cdot \boldsymbol{n}$ through the free surface

$$\frac{d\eta}{dt} = \frac{df}{dn_y}. \tag{4}$$

A finite volume code employing a cell-centered variable layout on general curvilinear grids has been extended by the arbitrary Lagrangian Eulerian (ALE) formulation [1] expressing the discretized mass and momentum balance equations on a time-varying grid in a conservative formulation. The elevation η is discretized at every grid cell face along the free surface, and (4) is then integrated in time by an explicit Adam Moulton third order multistep method. An adaptive curvilinear grid is generated algebraically and the time integration of the fluid motion is performed by a second order fractional step method, to some extend following Zang et al. (1994) [5]. Assuming that solutions for velocity and pressure exist up to time step t^n, and grid and boundary conditions have been set for t^{n+1}, the velocity field at time t^{n+1} is split into a predictor velocity field $\boldsymbol{u}^*$ and an irrotational correction $\nabla\phi$,

$$\boldsymbol{u}^{n+1} = \boldsymbol{u}^* + \nabla\phi. \tag{5}$$

$\boldsymbol{u}^*$ is updated by time-integrating to second order the momentum equations (2)

$$\begin{aligned} \frac{\boldsymbol{u}^* - \boldsymbol{u}^n}{\Delta t} &+ \frac{1}{2}((\boldsymbol{u}_g(\nabla \boldsymbol{u}^*) + \boldsymbol{u}_g(\nabla \boldsymbol{u}^n)) \\ &= \frac{3}{2}\nabla p^n - \frac{1}{2}\nabla p^{n-1} \\ &- \frac{3}{2}(\boldsymbol{u}(\nabla \boldsymbol{u}))^n - \frac{1}{2}(\boldsymbol{u}(\nabla \boldsymbol{u}))^{n-1}, \end{aligned} \tag{6}$$

employing QUICK interpolation for the convective terms. The grid velocity $\boldsymbol{u}_g$ reflects the motion of grid lines from time step n to $n+1$ according to the ALE approach. The correction $\nabla\phi$ is determined by restricting $\boldsymbol{u}^{n+1}$ to satisfy the continuity equation (1), hence

$$\nabla^2\phi = -\nabla \boldsymbol{u}^*. \tag{7}$$

The pressure is computed by the divergence of the momentum equation (2)

$$\nabla^2 p^{n+1} = -\nabla \cdot (\boldsymbol{u} \cdot \nabla \boldsymbol{u})^{n+1}, \tag{8}$$

together with boundary condition (3). While the implicit part of the discretized momentum equation (6) is solved iteratively by either point- or line-relaxation, the Poisson equations (7) and (8) are solved by a standard multigrid method.

Waves are generated by imposing second order Stokes velocity profiles at one side of the fluid domain of the form

$$u_x = (U_1(y)\sin(\varphi) + U_2(y)\sin(2\varphi)), \qquad (9)$$

with $\varphi = \omega t + \theta$. At the opposite end both the elevation η and the fluid velocity $\boldsymbol{u}$ are relaxed at every timestep towards prescribed values, η_p and $\boldsymbol{u}_p$, respectively, by following procedure

$$\eta = (1-\alpha)\eta + \alpha\eta_p\ ,\ \ \boldsymbol{u} = (1-\alpha)\boldsymbol{u} + \alpha\boldsymbol{u}_p. \quad (10)$$

α denotes a relaxation parameter, which increases softly as the waves are entering into the numerical sponge layer.

Results. The method has been tested for standing and travelling waves in both deep and shallow water. With numerical resolutions in time and space of $L/\Delta x >= 50$ and $T/\Delta t >= 50$, respectively, the linear dispersion relation is fulfilled to an accuracy better than 1%. Errors in mass conservation can be neglected in all cases, because the kinematic condition is expressed in terms of the local volume flux and the discretization of the transport equations is conservative. However, since in contrast to potential flow methods, no energy equation is solved, but energy balance has to emerge out of the numerical solution of mass and momentum transport equations, the main problem are errors in energy conservation. With a resolution of $L/\Delta x \approx 50$ and $T/\Delta t \approx 50$ about 0.5% of the energy of a deep water standing wave is dissipated during a wave period. Using $L/\Delta x \approx 50$ and $T/\Delta t \approx 100$ that number is decreased to about 0.1%.

The method has been used to study the propagation of regular incident waves with period $T = 2.02$ s and height $H = 0.02$ m over a submerged bar on a horizontal bottom, see Fig. 1, this test being investigated experimentally by Luth et al. (1994) [2]. On the upward slope the incoming waves are shoaling, nonlinearity hereby generating bound higher harmonics, which travel phase locked to the primary wave. On the downward slope these harmonics are released as free waves resulting in an irregular wave pattern.

In the simulation waves are generated for 80 s in fluid initially being at rest. The computed elevation history and its Fourier transform has been compared to measurements at selected locations, see Figs. 2 and 3. On the upward slope good agreement with measurements is found, the nonlinear shoaling process being well described even with rather coarse discretization. On the lee side of the bar fine spatial discretization is required to resolve the released higher harmonic waves, which are otherwise damped by numerical dissipation. However, given sufficient discretization, the model describes phase accurate the resulting irregular wavetrain behind the bar.

In a channel with a submerged bar a steady current is introduced by modifying the sponge layer and the wave generating boundary condition, see Fig. 4. The local Froude number on top of the bar takes values of about $Fr \approx 0.4$. Waves of height $H = 0.005$ m and with periods $T = 2$ s and $T = 1$ s, respectively, are generated during 100 s and propagate against the mean flow direction. In the case, $T = 2$ s waves travel in close agreement with linear theory with regard to amplitude and wave number, almost recovering to their initial shape after the bar, see Fig. 5.

In the case of $T = 1$ s, however, waves are blocked on the upward slope, since the current velocity exceeds the group velocity of the wave. The blocking point agrees precisely to the location estimated by linear wave theory. In order to resolve more closely the blocking process, discretization is refined to $\Delta t = 0.005$ s and $\Delta x \approx 0.01$ m around the blocking point and waves with initial heights of both $H = 0.001$ m and $H = 0.005$ m are generated. The elevation profile clearly shows the incoming wave to be superposed by short reflected waves, with wavelength being shortened with increasing depth and dissipated by numerical damping, see Fig. 6.

Integral mass and energy equations can be solved to estimate the mean velocity U and the mean elevation η_m as function of the horizontal position x. The expression for the apparent frequency

$$\sigma = \omega + kU\ ,\ \ \sigma = 2\pi/T, \qquad (11)$$

can then be solved together with the linear dispersion relation,

$$\omega^2 = gk\tanh k(h+\eta_m), \qquad (12)$$

having two solutions for k, the smaller k_i being the wave number of the Doppler shifted incident wave, and the greater k_r being the wave number of the reflected wave, if blocking occurs, see e.g. [3].

By identifying the wave crests in the computed elevation profile $\eta(x)$, or the vertical fluid velocity $u_y(x)$, respectively, the wave number of the reflected wave is estimated as function of x, see Fig. 8. The estimated wave numbers are seen to be scattered, but found in average to follow quite closely the theoretical estimate. The scattering increases with the increasing initial height of the generated wave, and seems to be due to the Doppler shift, by which the incident waves influence the shorter reflected waves.

Conclusion A finite volume code employing a modified fractional step method has been applied to

unsteady, incompressible free-surface flow. The numerical damping characteristics are not good compared to state of the art potential flow methods using equivalent resolution in time and space. However, the numerical accuracy in the present method is sufficiently good to allow phase-accurate simulation of nonlinear 2D waves within $O(100)$ wave lengths or wave periods, which we believe is an improvement compared to results in the past. Both steady and non steady rotational currents can be introduced directly, the example of wave blocking being a demonstration of the special capabilities of the present method.

The method is intended to be a supplement for investigation of interaction of wave motion with other processes as wave-current interaction, interaction with laminar and turbulent bottom boundary layers, etc. Finally, we believe that the present method is a good basis on which models describing the effect of wave breaking on wave driven currents, turbulence, etc., can be developed.

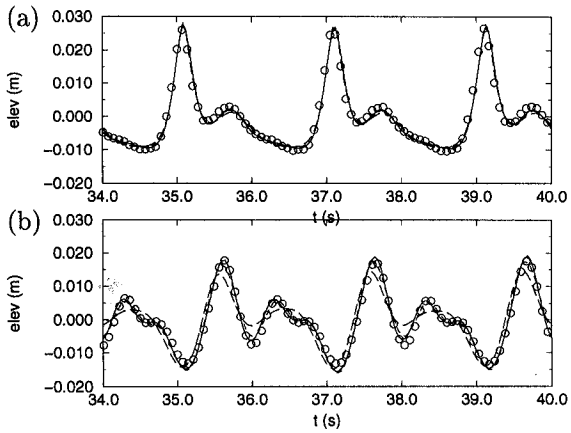

Figure 2: Surface elevations as funtion of time of waves propagating over submerged bar, see Fig. 1. (a) $x = 13.5$ m (top of bar), (b) $x = 21$ m, (behind bar). (o) meas., Luth et al. (1994), (----) comp., $\Delta x = 0.015$ m, $\Delta t = 0.01$ s, (- - - -) comp., $\Delta x = 0.03$ m, $\Delta t = 0.02$ s, (-- -- --) comp., $\Delta x = 0.06$ m, $\Delta t = 0.04$ s.

References

[1] R. K. C. Chan. *J. Comput. Phys.*, 17:311–331, 1975.

[2] H. R. Luth, G. Klopman, and N. Kitou. Technical Report H1573, Delft Hydraulics, 1994.

[3] D. H. Peregrine. *Adv. in Appl. Mech.*, 16:10–117, 1976.

[4] W. Tsai and D. K. P. Yue. *Ann. Rev. Fluid. Mech.*, 28:249–78, 1996.

[5] Y. Zang, R. L. Street, and J. R. Koseff. *J. Comput. Phys.*, 114:18–33, 1994.

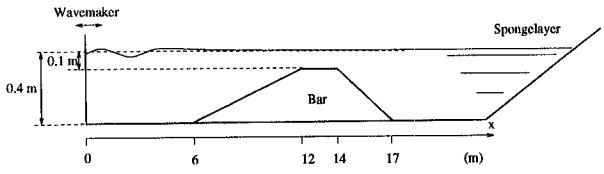

Figure 1: Wave Flume with submerged bar on horizontal bottom. Waves are generated with inital height $H = 0.02$ m and period $T = 2.02$ s.

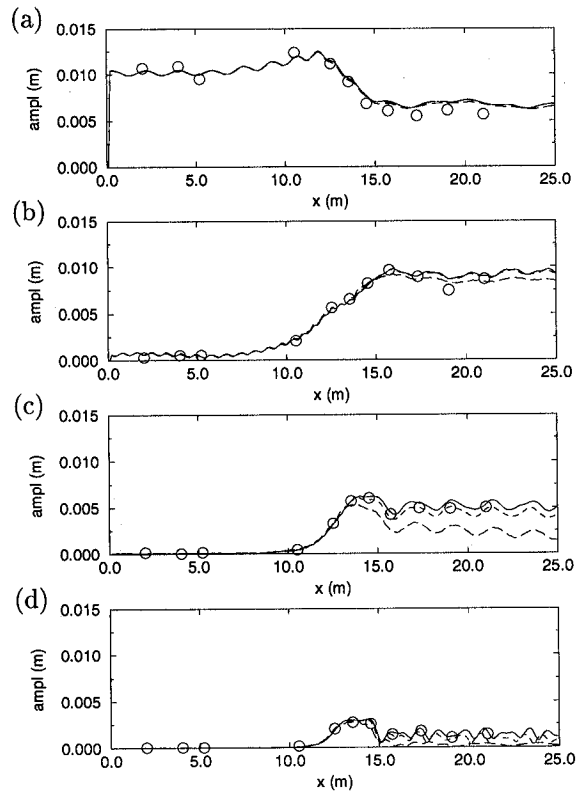

Figure 3: Propagation of regular waves over a submerged bar, see Fig. 1. (a-d) Amplitudes of 1^{st} to 4^{th} harmonic, respectively, as function of x-location along the channel. (o) measurements by Luth et al. (1994), (----) $\Delta x = 0.015$ m, $\Delta t = 0.01$ s, (- - - -) $\Delta x = 0.03$ m, $\Delta t = 0.02$ s, (-- -- --) $\Delta x = 0.06$ m, $\Delta t = 0.04$ s.

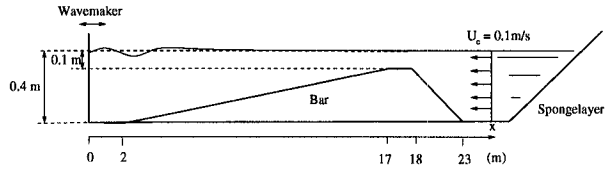

Figure 4: Wave Flume with submerged bar on horizontal bottom for studying wave current interaction.

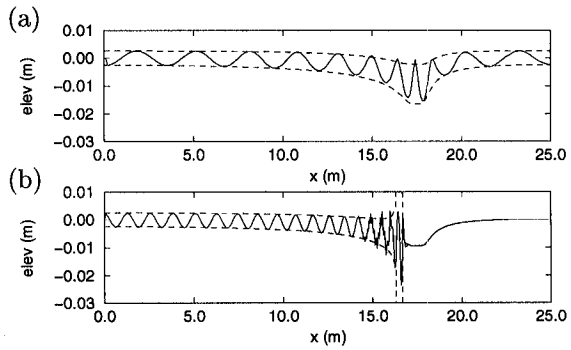

Figure 5: Propagation of waves over a submerged bar with opposing current, see Fig. 4. Elevation profiles at 5 phases within a period at $t = 95$ s. Initial wave height, $H = 0.005$ m, and current $U_c = 0.1$ m/s at 0.4 m depth. (a) Wave period $T = 2$ s. (b) Wave period $T = 1$ s. (- - - -) envelope according to linear wave theory.

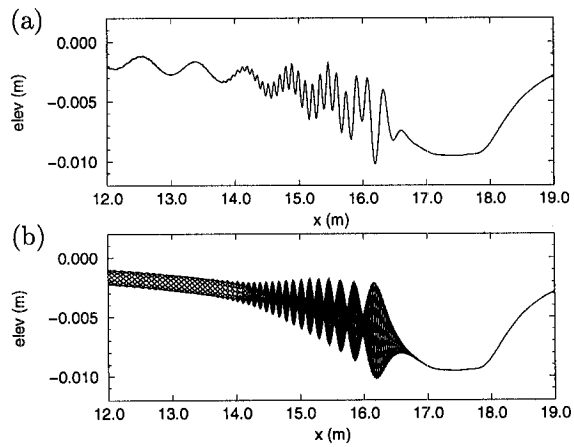

Figure 6: Wave with period $T = 1$ s and initial height $H = 0.001$ m propagating against steady current, see Fig. 4. (a) Elevation at $t = 95$ s. (b) Elevation profiles at 10 phases within a period bewteen $t = 95$ s and $t = 96$ s.

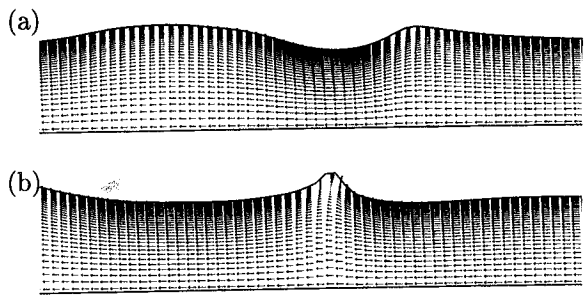

Figure 7: Fluid domain and velocity vectors around blocking point of waves with period $T = 1$ s and initial height $H = 0.005$ m propagating against steady current, see Fig. 4. (a) $t = 95.00$ s, (b) $t = 95.50T$ s.

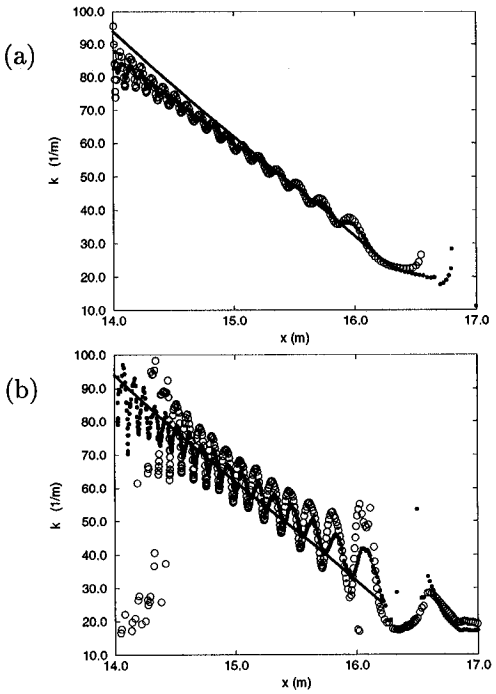

Figure 8: Estimate of wavenumber of wave, being reflected by current, as function of the location x. (a) initial wave height $H = 0.001$ m, (b) initial wave height $H = 0.005$ m. (o) estimate based on surface elevation, (·) estimate based on vertical surface velocity, (----) theoretical value based on (11) and (12).

DISCUSSION

Borthwick A.: Is the algebraically generated curvilinear grid essentially the same as a sigma transformed mesh? If so, could not additional savings in computer time be gained by using the sigma transformed approach given that the mapped equations would be simpler?

Mayer S.: Since the code is derived from a general purpose CFD code, the Finite Volume discretization scheme is implemented for general non-orthogonal grids, including cross derivative terms in both the interior of the grid and along grid boundaries.
However, the automatic grid generation algorithms used in the present work are almost equivalent with the use of sigma transformed meshes, since the considered geometries are simple and, in particular, the channel side walls are vertical. In general, both memory requirement and CPU-consumption could probably be reduced quite a lot, if our algorithm would be written specifically for the numerical wave flume application. This is not only due to the possible simplification of grid generation and discretization schemes, but also because the solution algorithm for the algebraic equation systems could take advantage of the simple grid structure.

Schultz W.W.: Does most of your numerical dissipation come from the Euler prediction step or the potential correction step?

Mayer S.: Generally, most numerical damping comes from the predictor step, in particular, from the QUICK upwind schemes, which we employ for the convective terms. Additionally, some dissipation is introduced in the spatial discretization of the kinematic boundary condition. For time steps, used here, the dissipation due to the potential correction is negligible. (However, for very small timesteps - 1000 time steps or more per wave period - it may become significant).